UCLA
UCLA Previously Published Works

Title

Analysis of plasmaspheric hiss wave amplitudes inferred from low-altitude POES electron data: Technique sensitivity analysis

Permalink

https://escholarship.org/uc/item/6rv6n014

Journal

Journal of Geophysical Research A: Space Physics, 120(5)

ISSN

2169-9380

Authors

De Soria-Santacruz, M
Li, W
Thorne, RM
et al.

Publication Date

2015-05-01

DOI

10.1002/2014JA020941

Peer reviewed

eScholarship.org Powered by the California Digital Library
University of California

AGU PUBLICATIONS

JGR

Journal of Geophysical Research: Space Physics

RESEARCH ARTICLE
10.1002/2014JA020941

Key Points:
- Inferred amplitudes are very sensitive to frequency spectrum and plasma density
- All estimates remain within a factor of 0.48 to 2.09 of the observed hiss waves
- Statistical frequency spectra should be used instead of standard Gaussian models

Correspondence to:
M. de Soria-Santacruz,
mdesoria@atmos.ucla.edu

Citation:
de Soria-Santacruz, M., et al. (2015), Analysis of plasmaspheric hiss wave amplitudes inferred from low-altitude POES electron data: Technique sensitivity analysis, *J. Geophys. Res. Space Physics*, *120*, 3552–3563, doi:10.1002/2014JA020941.

Received 11 DEC 2014
Accepted 12 APR 2015
Accepted article online 16 APR 2015
Published online 15 MAY 2015

©2015. American Geophysical Union. All Rights Reserved.

Analysis of plasmaspheric hiss wave amplitudes inferred from low-altitude POES electron data: Technique sensitivity analysis

M. de Soria-Santacruz[1,2], W. Li[2], R. M. Thorne[2], Q. Ma[2], J. Bortnik[2], B. Ni[3], C. A. Kletzing[4], W. S. Kurth[4], G. B. Hospodarsky[4], H. E. Spence[5], G. D. Reeves[6], J. B. Blake[7], and J. F. Fennell[7]

[1]University Corporation for Atmospheric Research, Boulder, Colorado, USA, [2]Department of Atmospheric and Oceanic Sciences, University of California, Los Angeles, California, USA, [3]Department of Space Physics, School of Electronic Information, Wuhan University, Wuhan, Hubei, China, [4]Department of Physics and Astronomy, University of Iowa, Iowa City, Iowa, USA, [5]Institute for the Study of Earth, Oceans, and Space, University of New Hampshire, Durham, New Hampshire, USA, [6]Space Science and Applications Group, Los Alamos National Laboratory, Los Alamos, New Mexico, USA, [7]The Aerospace Corporation, Los Angeles, California, USA

Abstract A novel technique capable of inferring wave amplitudes from low-altitude electron measurements from the Polar Operational Environmental Satellites (POES) spacecraft has been previously proposed to construct a global dynamic model of chorus and plasmaspheric hiss waves. In this paper we focus on plasmaspheric hiss, which is an incoherent broadband emission that plays a dominant role in the loss of energetic electrons from the inner magnetosphere. We analyze the sensitivity of the POES technique to different inputs used to infer the hiss wave amplitudes during three conjunction events with the Van Allen Probes. These amplitudes are calculated with different input models of the plasma density, wave frequency spectrum, and electron energy spectrum, and the results are compared to the wave observations from the twin Van Allen Probes. Only one parameter is varied at a time in order to isolate its effect on the output, while the two other inputs are set to the values observed by the Van Allen Probes. The results show that the predicted hiss amplitudes are most sensitive to the adopted frequency spectrum, followed by the plasma density, but they are not very sensitive to the electron energy spectrum. Moreover, the standard Gaussian representation of the wave frequency spectrum (centered at 550 Hz) peaks at frequencies that are much higher than those observed in individual cases as well as in statistical wave distributions, which produces large overestimates of the hiss wave amplitude. For this reason, a realistic statistical model of the wave frequency spectrum should be used in the POES technique to infer the plasmaspheric hiss wave intensity rather than a standard Gaussian distribution, since the former better reproduces the observed plasmaspheric hiss wave amplitudes.

1. Introduction

Plasmaspheric hiss is an incoherent and structureless whistler mode emission commonly observed in the high-density regions of the magnetosphere, namely, the plasmasphere and the dayside plasmaspheric plume [*Meredith et al.*, 2006]. Hiss waves are responsible for the formation of the slot region that appears between the inner and outer radiation belts [*Lyons and Thorne*, 1973; *Abel and Thorne*, 1998]. Plasmaspheric hiss is also associated with the scattering of energetic outer belt electrons during geomagnetically active times [*Summers et al.*, 2008; *Ni et al.*, 2014a] and the slow decay of the outer Van Allen belt that follows geomagnetic storms [*Meredith et al.*, 2006, 2007, 2009; *Baker et al.*, 2007; *Thorne et al.*, 2013]. Plasmaspheric hiss plays an important role in the dynamics of the inner magnetosphere, and for this reason it is important to understand and model its structure and interaction with the energetic electron population, hence building the path toward reaching predictive capabilities of its behavior. Current modeling techniques use quasi-linear theory [*Kennel and Petschek*, 1966] to calculate the diffusion of energetic particles caused by magnetospheric waves. These codes require input models of the wave properties, which have a strong impact on the results. Statistics of in situ wave observations are commonly used to build these models, which are based on data with limited coverage and for this reason may not be capable of reproducing the instantaneous global wave distribution in the magnetosphere. In the case of hiss, statistical models exist based on Combined Release and Radiation Effects Satellite (CRRES) data [*Meredith et al.*, 2004; *Orlova et al.*, 2014], which have been extensively used to estimate the effect of hiss waves on the dynamics of radiation belt electrons [e.g., *Meredith et al.*, 2007]. Moreover,

Li et al. [2015] present a new statistical study of plasmaspheric hiss based on Van Allen Probes data, which will be used in the analysis presented in this paper.

More recently, an alternative physics-based technique has been proposed, which is capable of inferring wave amplitudes from low-altitude electron data taken by the Polar Operational Environmental Satellites (POES). Compared to in situ wave measurements by near-equatorial satellites alone, this technique provides broad coverage in L shell and magnetic local time (MLT) due to the short orbital period (~100 min) and high inclination (~98°) of the multiple POES spacecraft. *Li et al.* [2013a] used this methodology to infer chorus wave amplitudes and compared them with wave observations from the Van Allen Probes during conjunction events, which agreed reasonably well; they concluded that the technique could therefore be used to provide global, real-time estimates of the chorus wave intensity. *Chen et al.* [2014b] also estimated the global time-dependent distribution of chorus waves using a heuristic formula that relates POES precipitating electron fluxes to the chorus intensity; the expression is derived from statistical distributions and scaled to in situ measurements from the Van Allen Probes. In a later paper, *Li et al.* [2014] analyzed a specific conjunction between POES and the Van Allen Probes where plasmaspheric hiss waves were observed, and they showed that the technique in *Li et al.* [2013a] is also able to reproduce the hiss wave intensity very well, which could potentially be used to infer its spatiotemporal evolution. *Ni et al.* [2014b] carefully described the physical processes behind the POES methodology and presented the details of its formulation. More specifically, the technique uses the precipitating and trapped electron fluxes measured by the Medium Energy Proton and Electron Detectors (MEPEDs) on board the POES spacecraft to infer the wave intensity. MEPED consists of two solid-state particle detectors, which are part of the Space Environment Monitor version 2 instrument package. One of the detectors is centered along the local zenith pointing outward and measures precipitating electrons at $L > 1.4$, while the second detector is oriented perpendicular to the former and measures a mixture of particles trapped between an invariant latitude of 55°–68° [*Meredith et al.*, 2011] as well as particles in the bounce and drift loss cones. Both detectors have a field of view of ±15° and measure electrons in three integral channels with energies >30 keV, >100 keV, and >300 keV. The essential concept of this technique is to use the ratio between the precipitating (J_0) and trapped (J_{90}) electron fluxes measured by POES as a sole function of the wave magnetic field amplitude, the expression of which was described in detail in previous publications [*Li et al.*, 2013a; *Ni et al.*, 2014b]. This expression involves calculation of the pitch angle diffusion coefficient as a function of wave amplitude, which requires assumptions for several free parameters: plasma density, wave frequency spectrum, and wave normal distribution. Similarly, the expression depends on the electron energy spectrum, which also has to be assumed. In this manuscript we focus on plasmaspheric hiss waves and aim to deepen our understanding by quantifying the sensitivity of the inferred wave amplitudes to different values of those free parameters. For this purpose, we analyze multiple conjunction events between POES and the Van Allen Probes where plasmaspheric hiss waves were observed by the Electric and Magnetic Field Instrument Suite and Integrated Science (EMFISIS) instruments [*Kletzing et al.*, 2014]. The sensitivity is studied by calculating wave amplitudes using the POES technique under different inputs, which we choose based on their observed values, analytical models, or statistical representations.

The following section describes the selected conjunction events between the POES and the Van Allen Probes spacecraft that are studied in this manuscript. The different models and observations of the input parameters are presented in section 3, and the resulting wave amplitudes inferred with the POES technique are described and analyzed in section 4. The paper concludes with a summary and discussion of the results.

2. Selected Conjunction Events

The sensitivity of the POES technique to the plasma density, wave frequency spectrum, and electron energy spectrum is studied for three conjunction events between the POES spacecraft (consisting of MetOp-2, NOAA 15, NOAA 16, NOAA 17, NOAA 18, and NOAA 19) and the Van Allen Probes (consisting of RBSP-A and RBSP-B) where plasmaspheric hiss waves were observed. A conjunction corresponds to an encounter between a POES and an RBSP spacecraft in the same bin of dimensions 0.5 h (UT) by 0.5 L shell by 0.5 h (MLT). The bins of the selected conjunction events are detailed in Table 1, where the UT, L shell, and MLT values represent the beginning of each bin. All the events are reasonably stable and occur during moderate geomagnetic conditions ($-100 > AL^* > -500$ nT, where AL^* is the minimum AL in the preceding 3 h) where the Earth's magnetic field geometry in the region of interest remained close to dipolar. The events occurred inside the plasmasphere; the location of the plasmapause was determined from the electric field spectral density measured by the EMFISIS instruments, which allowed us to (1) obtain the electric field in the electron cyclotron harmonic

Table 1. Selected Conjunction Events[a]

Event	Day	UT (h)	*L* Shell	MLT (h)	Satellites
1	23 Oct 2012	06:00:00	4.5	4.5	RBSP-B and NOAA 17
2	23 Dec 2012	12:00:00	5.0	6.0	RBSP-A and NOAA 15
3	11 Feb 2014	00:30:00	4.5	13.5	RBSP-A and NOAA 18

[a]UT, *L* shell, and MLT values represent the beginning of the corresponding bins.

(ECH) range by integration of this spectrum [*Meredith et al.*, 2004] and (2) obtain the plasma density from the upper hybrid line observed in the same spectrum [*Kurth et al.*, 2015]. The inferred density can be calculated as $n_e = \left(f_{uh}^2 - f_{ce}^2\right)(2\pi)^2 \epsilon_0 m_e/q^2$, where m_e is the electron mass, q is the electron charge, f_{ce} is the electron cyclotron frequency obtained from Van Allen Probes data, and f_{uh} corresponds to the upper hybrid line in the spectrum. Those intervals with electric field smaller than 10^{-6} V/m (since ECH waves are weak inside the plasmasphere) and plasma density larger than max[50,$(6.6/L)^4$] cm^{-3} [*Li et al.*, 2010, equation (1)] were considered inside the plasmasphere.

Additionally, magnetosonic waves were excluded from the analysis during the corresponding time intervals; specifically, we removed those measurements with |ellipticity| < 0.2 and wave normal angle $>80°$ [*Horne et al.*, 2007], which are directly provided by level 4 data from the EMFISIS instruments calculated based on three components of magnetic field measurements using the singular value decomposition method [*Santolik et al.*, 2003].

The first selected event corresponds to a conjunction between RBSP-B and NOAA 17 which occurred on 23 October 2012 at 6:00:00 UT; during this time, RBSP-B was crossing $L = 4.5$ and orbiting on the nightside around MLT $= 4.5$ h. Figure 1a presents the instantaneous *AL* index during this event, the minimum of which was $AL^* = -250$ nT in the last 3 h. The magnetic field spectral density measured by the waveform receiver (WFR) shown in Figure 1b is concentrated between 50 Hz and 500 Hz, and Figure 1c shows that the wave magnetic field (calculated by integrating the spectral density between 20 Hz and 2 kHz) exceeds 100 pT and remains stable throughout the entire period. The lower hybrid and electron cyclotron frequencies are indicated by the white and green lines of Figure 1b, respectively. The electric field spectral density measured by the high-frequency receiver (HFR) is also presented in Figure 1d, which is used to obtain the wave electric field and to infer the plasma density from the observed upper hybrid line as described above. Figure 1e presents the flux of trapped (black) and precipitated (red) electrons with energies >100 keV measured by the MEPED instrument on the POES spacecraft, which shows that the slot region was filled with high-energy electrons during this period; the shaded time interval corresponds to the conjunction with RBSP-B, namely, the location in the NOAA 17 orbit where the spacecraft is in the same *L* shell and MLT bin as RBSP-B. Similarly, the second event is summarized in Figures 1f–1j, which corresponds to a conjunction between RBSP-A and NOAA 15 on 23 December 2012 at 12:00:00 UT. At that time RBSP-A was crossing $L = 5$ in the dawn sector. For this event the geomagnetic activity was also moderate with $AL^* = -170$ nT. The most remarkable aspect of the event, however, is revealed by the frequency spectrogram in Figure 1g, which shows that the wave magnetic field spectral density peaks at frequencies below ~80 Hz, much lower than the typical hiss wave frequency [*Thorne et al.*, 1973; *Meredith et al.*, 2004]. These very low frequency hiss events, however, are indeed quite common as shown by recent statistical studies based on EMFISIS data [*Li et al.*, 2015]. The CRRES spacecraft was not capable of observing these features because the lowest frequency covered by the sweep frequency receiver was 100 Hz. Additionally, CRRES was only capable of measuring the wave electric field, while the magnetic field was calculated by assuming parallel wave propagation; the hiss wave normal angle, however, can be very variable [*Parrot and Lefeuvre*, 1986; *Santolik et al.*, 2001]. With the Van Allen Probes, however, we are capable of detecting these very low frequency events without ambiguity thanks to EMFISIS's broader frequency coverage and its ability to measure both electric and magnetic fields, which allow us to calculate the wave normal angle and polarization properties and therefore distinguish plasmaspheric hiss from other types of waves, such as magnetosonic waves. Finally, the third event is presented in Figures 1k–1o, which corresponds to a conjunction between RBSP-A and NOAA 18 on 11 February 2014 at 00:30:00 UT and at $L = 4.5$ on the dayside. The geomagnetic activity was also moderate with $AL^* = -441$ nT, and in contrast to the previous event, the peak frequency of this conjunction lays within the standard range for plasmaspheric hiss. Figures 1e, 1j, and 1o show

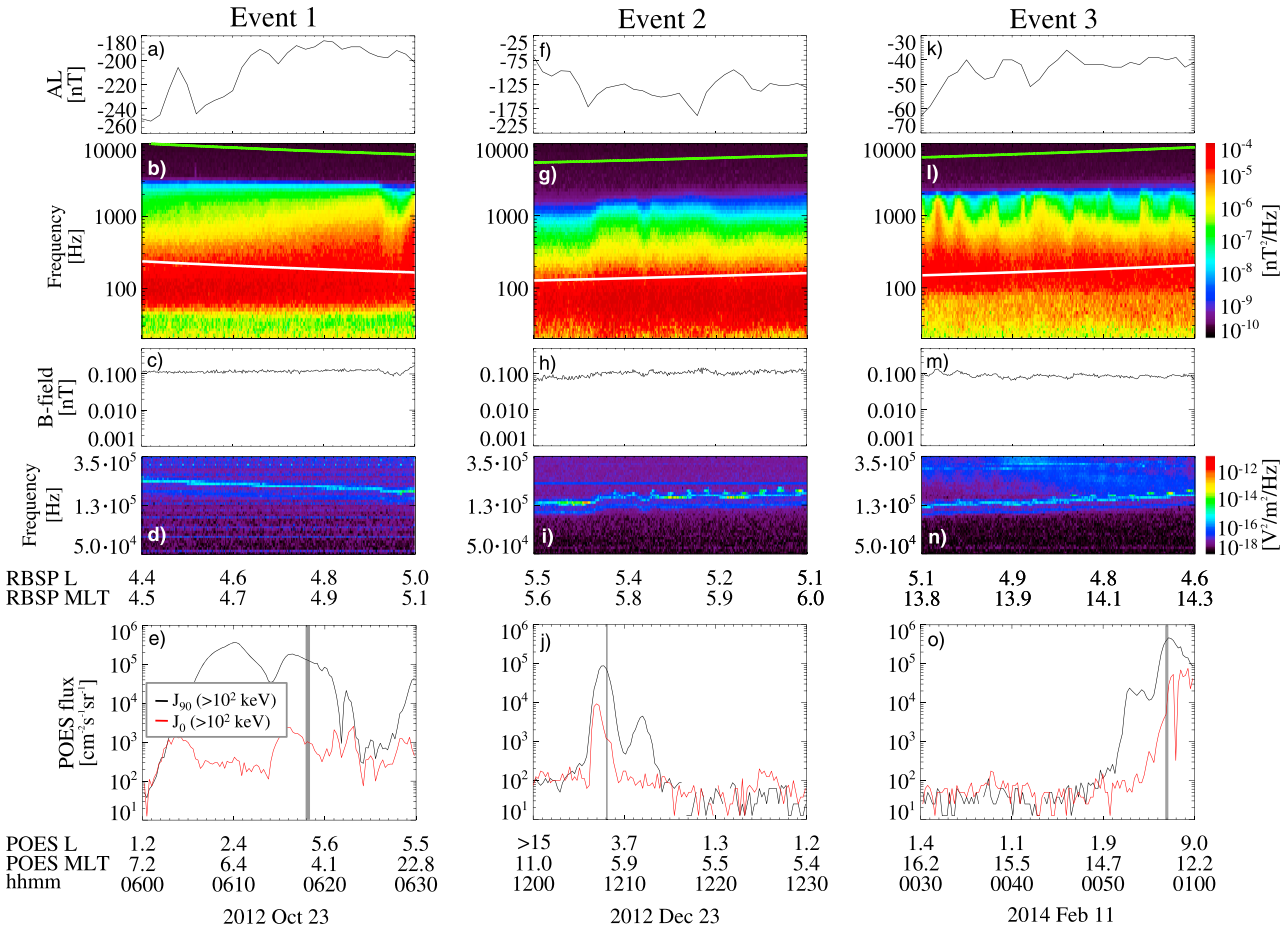

Figure 1. (a) *AL* index of event 1. (b) Frequency-time spectrogram of the magnetic field spectral density from the WFR channel for event 1; the white and green lines represent the lower hybrid and electron cyclotron frequencies, respectively. (c) Plasmaspheric hiss magnetic wave amplitude for event 1. (d) Frequency-time spectrogram of the electric field spectral density from the HFR channel for event 1. Figures 1b–1d correspond to Van Allen Probes observations from the EMFISIS instrument. (e) Trapped and precipitated electron fluxes measured by the POES spacecraft in the >100 keV channel for event 1; the shaded time interval within the POES orbit corresponds to the conjunction slot with the RBSP satellite. (f–j) The same as Figures 1a–1e but for event 2. (k–o) The same as Figures 1a–1e but for event 3.

that the precipitated fluxes of the selected events over the conjunction bins are above 1000 cm^{-2} s^{-1} sr^{-1}, that is, relatively high fluxes.

The inferred wave amplitudes are calculated from electron fluxes with energies between 100 keV and 300 keV, since it has been shown that this is the range that provides more reliable and robust results when inferring the plasmaspheric hiss wave amplitudes from electron precipitation [*Meredith et al.*, 2004; *Li et al.*, 2014]. These fluxes are obtained by subtracting the >300 keV from the >100 keV integral channels of the MEPED detectors, whose orientation with respect to the Earth's magnetic field is *L* shell dependent [*Rodger et al.*, 2010]. The technique needs precipitating fluxes above the background level (we set the threshold at >500 cm^{-2} s^{-1} sr^{-1}) in order to provide reliable results, which are typically observed in the outermost part of the plasmasphere. Although the slot region can be filled with energetic electrons particularly during disturbed periods [e.g., *Zhao and Li*, 2013], the trapped and precipitating fluxes of high-energy electrons in the slot region are generally very low. For this reason the POES technique tends to show a better performance at relatively large *L* shells within the plasmasphere for the majority of the events. All the hiss events that we selected occurred at $L > 4$, where the POES count rates were sufficiently high to provide reliable predictions of the wave amplitudes for realistic input parameters. Additionally, *Li et al.* [2013b] noted that very low frequency plasmaspheric hiss waves similar to the ones in event 2 may only be amplified in the outer part of the dayside plasmasphere (large *L* shells), since injected energetic electrons were suggested as their generation mechanism, as recently modeled by *Chen et al.* [2014a].

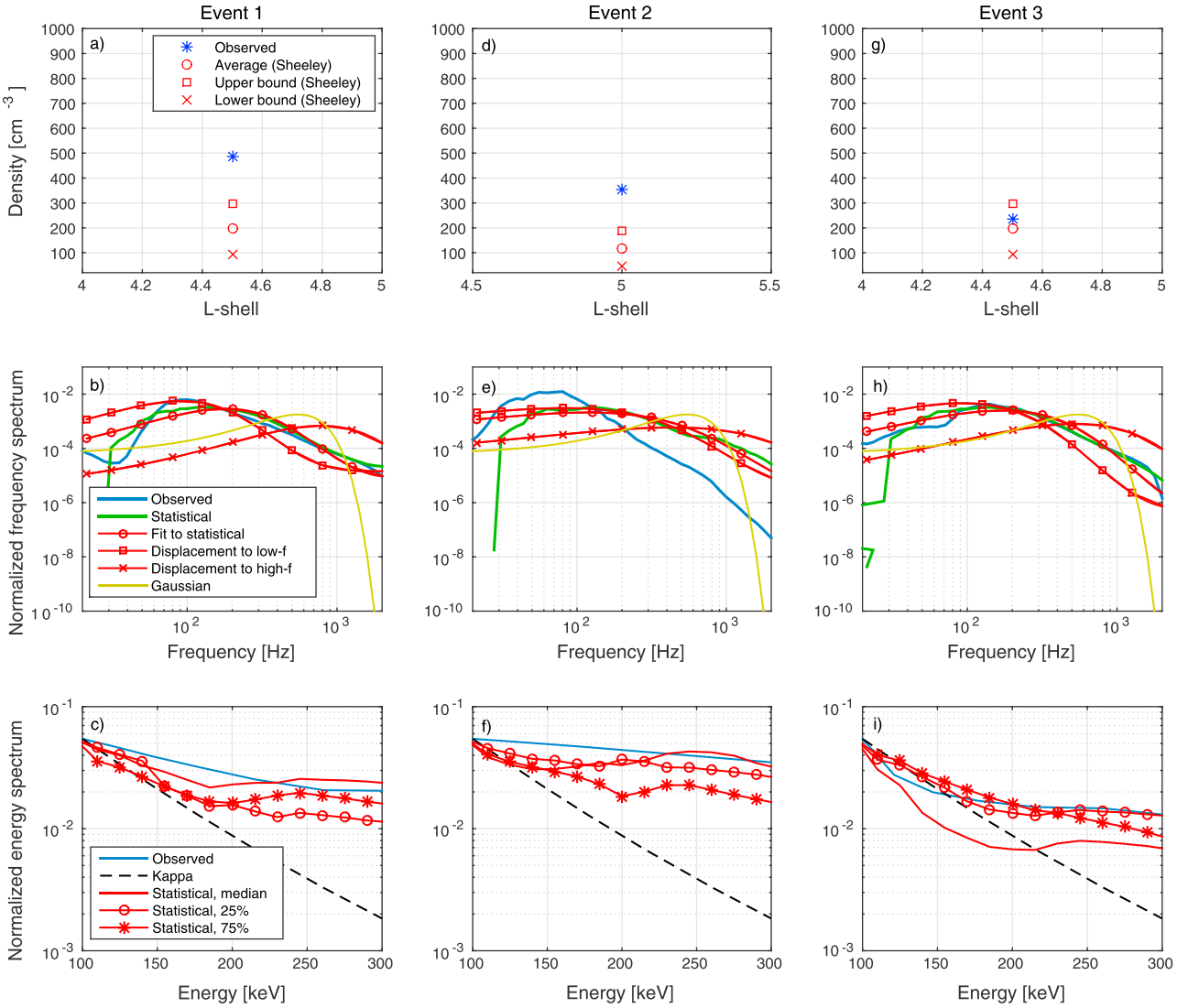

Figure 2. (a) Observed and modeled cold plasma density for event 1. (b) Observed and modeled wave frequency spectra normalized to let them have an integrated wave power of 1 pT^2 for event 1. (c) Observed and modeled electron energy spectra normalized with the value of the observed spectra at 100 keV for event 1. (d–f) The same as Figures 2a–2c but for event 2. (g–i) The same as Figures 2a–2c but for event 3.

3. Modeling of the Input Parameters

The ratio between precipitating and trapped electrons is the key element of the POES technique, which can be expressed as a function of wave magnetic field intensity, cold plasma density, and the shape of the wave frequency and electron energy spectra [*Ni et al.*, 2014b]. For the events presented above we calculate the inferred hiss wave amplitudes using the POES technique and study its sensitivity by varying the inputs to the code over reasonable bounds. The cold plasma density is one of these inputs, which is used in the University of California, Los Angeles (UCLA), Full Diffusion Code [e.g., *Ni et al.*, 2008, 2011] to calculate the pitch angle diffusion coefficient that appears in the expression for the ratio between precipitating and trapped electron fluxes. More specifically, we consider four different values for the plasmaspheric density with the purpose of studying the sensitivity of the results to this parameter, which correspond to its observed value (averaged over the conjunction bin) obtained from the upper hybrid line in the electric field spectra of Figure 1, as well as an empirical representation based on CRRES data given by *Sheeley et al.* [2001] that provides average, upper bound (average plus standard deviation), and lower bound (average minus standard deviation) values as a function of *L* shell. Observed and modeled plasma density values are presented in Figures 2a, 2d, and 2g for

each of the events. All the observed plasma densities are above the average empirical estimate, and events 1 and 2 even exceed the upper bound value.

A second input to the calculation of the pitch angle diffusion coefficient is the wave magnetic field spectral density at various frequencies. The observed value used in the simulations corresponds to the average over the conjunction bin of the magnetic field density in the WFR spectrogram in Figure 1 as a function of frequency. A statistical representation of the frequency spectrum built from EMFISIS data is also studied, which is described in *Li et al.* [2015] and includes Van Allen Probes observations from 1 October 2012 to 1 October 2014. This statistical frequency spectrum is a function of L shell (bins of 0.5), MLT (4 h bins), and geomagnetic activity (quiet for $AL^* > -100$ nT, moderate for $-100 > AL^* > -500$ nT, and active for $AL^* < -500$ nT), and it has been obtained by averaging the observed spectrum over the 2 years of observations as a function of frequency in the specified bins. Moreover, we also test a standard Gaussian distribution centered at $f_c = 550$ Hz with $\Delta f = 300$ Hz and lower and upper cutoffs given by $f_{lc} = 20$ Hz and $f_{uc} = 4$ kHz, respectively. Additionally, the analysis in the following section studies the effect of moving the peak frequency toward lower and higher values. For this purpose, we have fitted the statistical data with a three-parameter analytical function (a, b, c), and we have slightly varied parameter b to displace the frequency peak from ~80 Hz to ~800 Hz while preserving the shape of the function. The fitted spectrum F_{fit} is given by

$$A = f^a e^{-f/b}, \quad B = 10^{Ac/\max(A)} \tag{1}$$

$$F_{fit} = \max\left(F_{stat}\right) \frac{B}{\max(B)} \tag{2}$$

where f is the frequency and F_{stat} is the statistical data. The fitting algorithm optimizes (a, b, c) by maximizing the coefficient of determination between the base 10 logarithm of the fitted function and the statistical frequency spectrum corresponding to the level of AL^* in each event. Figures 2b, 2e, and 2h show the six different representations of the frequency spectrum described above, which are compared in the following section. The curves named "Displacement to low-f" and "Displacement to high-f" were calculated by varying the b parameter of the fitted function within a reasonable range to achieve a peak frequency of ~80 Hz and ~800 Hz, respectively. Since it is only the shape of the curves that matters to the calculation of the diffusion coefficient and not their absolute value, we have normalized each frequency spectrum with its own integration over frequency between 20 Hz and 3.5 kHz.

It must be noted that the sensitivity to the wave normal angle is not analyzed in this paper but it is assumed Gaussian with a peak wave normal angle of 0° at the equator, which increases with latitude following Table 1 of *Ni et al.* [2013]. *Li et al.* [2014] showed that the POES technique applied to plasmaspheric hiss is relatively insensitive to the wave normal distribution, except when the waves are very oblique and close to their resonance cone. The wave normal angle observed by the Van Allen Probes in the selected events, however, remains below 40° (not shown), which is much smaller than the resonance cone angle of plasmaspheric hiss.

Finally, the electron energy spectrum also needs to be provided to calculate the plasmaspheric hiss intensity from POES electron data. The energy spectrum observed by the Van Allen Probes between 100 keV and 300 keV is taken from the Magnetic Electron Ion Spectrometer (MagEIS) [*Blake et al.*, 2013] of the Energetic Particle, Composition, and Thermal Plasma Suite (ECT) [*Spence et al.*, 2013]. Similar to the wave frequency spectrum, we use MagEIS data to construct a statistical model of the electron energy spectrum as a function of AL^*, L shell, and MLT (the same binning as for the frequency spectrum and also averaged over the conjunction bin) and we calculate the 25%, 50% (or median), and 75% percentiles. Additionally, a kappa function with parameters $\chi^2 = 0.05$ and $\kappa = 5$ [*Ni et al.*, 2014b, equation (9)] is also tested as proposed by *Xiao et al.* [2008]. These different representations of the energy spectrum are presented in Figures 2c, 2f, and 2i for the three different events. The curves have again been normalized with the maximum value of the observed energy spectra over the energy range of interest, which is the reason for the overlap and crossing of the different percentiles. This normalization provides a clearer visualization of the differences between models that are relevant to the calculation of the wave amplitudes.

4. Sensitivity of the Technique to the Input Parameters

For the three conjunction events described in section 2, we now calculate the inferred plasmaspheric hiss amplitudes using the POES technique with the different input parameters in section 3. We initially assign

Table 2. Sensitivity to Density[a]

Event	Density	Observed B_w (pT)	Inferred B_w (pT)	Difference (pT)	Ratio
1	Observed	119	87	−32	0.73
	Statistical average		57	−62	0.48
	Upper bound		65	−54	0.55
	Lower bound		63	−56	0.53
2	Observed	121	100	−21	0.83
	Statistical average		60	−61	0.50
	Upper bound		70	−51	0.58
	Lower bound		85	−36	0.70
3	Observed	85	81	−4	0.95
	Statistical average		74	−11	0.87
	Upper bound		90	5	1.06
	Lower bound		67	−18	0.79

[a]Statistical average, upper, and lower bounds from *Sheeley et al.* [2001]. Wave frequency spectrum and electron energy spectrum set to their observed values.

the observed values to all the inputs, and next we study the sensitivity to density, frequency spectrum, and electron energy spectrum by varying one parameter at a time (while the rest of the inputs are set to their observed values measured by the EMFISIS instruments). The results from the POES technique are compared to wave observations from the Van Allen Probes in the same conjunction bin.

4.1. Sensitivity to Density

Table 2 shows the effect on the inferred wave amplitude of varying the density model for the observed frequency and electron energy spectra. Both observed (by the EMFISIS wave instruments) and inferred (by the POES technique) wave amplitudes are included in the table, as well as their difference (inferred B_w − observed B_w) and ratio (inferred B_w/observed B_w).

For all three events the observed density input always provides the most accurate wave amplitudes. For the first event, the observed density (487 cm^{-3}) is above the upper statistical bound from *Sheeley et al.* [2001] (298 cm^{-3}), and all the density models (including the observed density input) underestimate the observed wave amplitude of 119 pT. Even though the lower statistical density bound (94 cm^{-3}) provides the worst amplitude estimate, it is still within a factor of 0.48 of its observed value. The behavior with density can be explained by looking at the pitch angle diffusion coefficient $D_{\alpha\alpha}$ for the four different density values, which are presented in Figure 3a. The figure shows that the peak of $D_{\alpha\alpha}$ moves to lower energies with increasing density; over the energy range of interest shaded in the figure (100 keV to 300 keV), this density dependence corresponds to a smaller diffusion coefficient for the case with observed density compared to the case with maximum density, and the latter corresponds to a smaller $D_{\alpha\alpha}$ than the case with average density. For fixed electron fluxes (given by the POES spacecraft), smaller diffusion coefficients result in larger inferred wave amplitudes, which explains the dependence on density of event 1 shown in Table 2. The behavior of the case with minimum density is not so easy to visualize, since the peak of its diffusion coefficient lies within the range of energies under consideration and goes across the other density cases, as shown in Figure 3a. Additionally, we should note that the peak in $D_{\alpha\alpha}$ is close to 100 keV so the effects on 100 to 300 keV electrons are even more sensitive. The maximum difference between models (best minus worst estimates) is a good way of quantifying the sensitivity of the technique to its inputs, which equals 30 pT for the first event. Similarly, for the second event, the observed density (353 cm^{-3}) is higher than the upper density bound from the Sheeley's model, and all the density inputs underestimate the observed wave amplitude (121 pT); this time, however, the worst performance model is the one with statistical average density, the amplitude estimation of which is only a factor of 0.5 smaller than the observed amplitude. The behavior with density of this event follows similar trends to that of event 1 in Figure 3a. The maximum absolute variation between models for the second event is 40 pT. Finally, the statistical representations of the density for the third event are close to its observed value, which was not the case for events 1 and 2. For this reason, the maximum absolute difference between models for event 3 is only 23 pT, and the worst of the models (minimum statistical density) only underestimates the observed amplitude (85 pT) by 27%, that is, a ratio of 0.79.

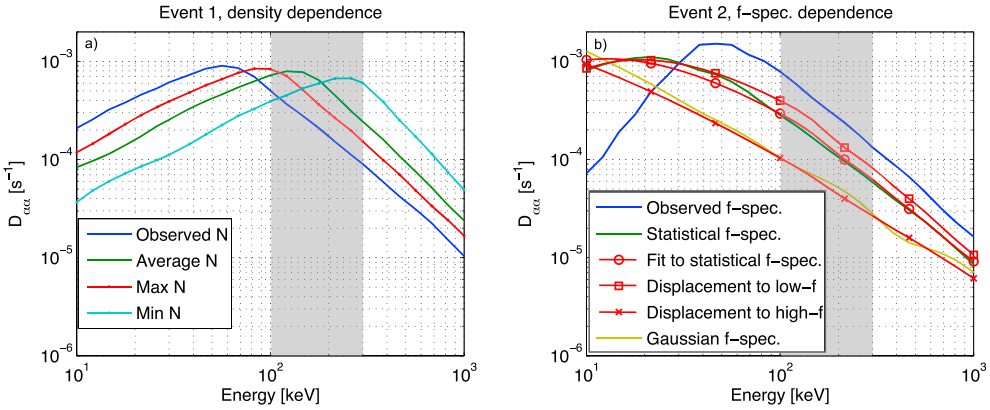

Figure 3. (a) Pitch angle diffusion coefficient at the bounce loss cone for event 1 ($L = 4.5$); the different curves correspond to different input plasma densities, while the frequency spectrum is set to its observed value. (b) Pitch angle diffusion coefficient at the bounce loss cone for event 2 ($L = 5$); the different curves correspond to different input wave frequency spectra, while the density is set to its observed value (353 cm^{-3}). Diffusion coefficients have been calculated using the UCLA Full Diffusion Code.

4.2. Sensitivity to Frequency Spectra

For this analysis we set the density and the energy spectra of 100 to 300 keV electrons to their observed values and we only vary the frequency spectra using the models described in section 3. The sensitivity to the wave frequency spectra is detailed in Table 3, which has the same format as Table 2.

The wave frequency in the first event peaks between 50 and 500 Hz, which lies within the standard frequency range attributed to plasmaspheric hiss waves as shown in Figure 1b. Therefore, the observed frequency spectrum, the statistical hiss wave spectrum from 2 years of Van Allen Probes wave data, and the analytical fitting to the statistics (equation (2)) provide good estimates of the wave amplitude, although all of them slightly underestimate its observed value. The Gaussian fitting overestimates the wave amplitude by 34% or a ratio of 1.34. The worst results come from the runs with displaced frequency spectra, that is, those where we moved

Table 3. Sensitivity to Frequency Spectra[a]

Event	*F* Spectra	Observed B_w (pT)	Inferred B_w (pT)	Difference (pT)	Ratio
1	Observed	119	87	−32	0.73
	Statistical		97	−22	0.82
	Fitting to statistical		103	−16	0.87
	Fit to high-*f* peak		201	82	1.69
	Fit to low-*f* peak		74	−45	0.62
	Gaussian		159	40	1.34
2	Observed	121	100	−21	0.83
	Statistical		160	39	1.32
	Fitting to statistical		154	33	1.27
	Fit to high-*f* peak		253	132	2.09
	Fit to low-*f* peak		132	11	1.09
	Gaussian		241	120	1.99
3	Observed	85	81	−4	0.95
	Statistical		81	−4	0.95
	Fitting to statistical		86	1	1.01
	Fit to high-*f* peak		145	60	1.71
	Fit to low-*f* peak		71	−14	0.84
	Gaussian		133	48	1.56

[a]Density and electron energy spectrum set to their observed values.

the peak frequency to the lower and higher values with respect to the statistical fitting. The worst performance ratio, however, is only 1.69, while the maximum absolute difference between models equals 127 pT.

The second event deviates from the commonly assumed features attributed to plasmaspheric hiss in that it spans a much lower frequency range, from 20 to 200 Hz as shown in Figure 1g. Figure 2e presents this aspect more clearly, which shows that the observed frequency spectrum (in dark blue) peaks at frequencies as low as 60 Hz; this frequency spectrum is not very well captured by the statistical model (in green) or by the fit to the statistics (in red). The sensitivity study of Table 3 details the effect of these different inputs, which shows that the observed frequency spectrum produces more accurate results than the statistical representation of the frequency spectrum. This statistical input, however, still estimates the hiss wave amplitude reasonably well, since it produces amplitude ratios no higher than 1.32. Another point to note is that the observed frequency spectrum slightly underestimates the wave amplitude while the statistical input overestimates it. The reason for this behavior stems from the dependence of the pitch angle diffusion coefficient on frequency, which is explained in Figure 3b. The statistical frequency spectrum peaks at higher frequencies than the observed spectrum due to the low-frequency nature of this event. However, in terms of the diffusion coefficient this has the opposite effect, since lower frequency hiss resonates with electrons with higher resonant energies as described by the hiss dispersion relationship and the resonance condition. In other words, the diffusion coefficient for the statistical frequency spectrum is displaced to lower energies compared to the one calculated with the observed frequency spectra, as shown in Figure 3b. For the energies of interest (100 keV to 300 keV), this implies a lower value of the diffusion coefficient for the statistical spectrum than for the observed spectrum. Since the precipitating fluxes are fixed (given by POES data), the smaller diffusion coefficient of the statistical frequency spectrum requires a larger wave amplitude to produce the same precipitation, which is the reason the statistical frequency spectrum overestimates the wave amplitude while the observed spectrum underestimates it. A similar analysis can be done for the fittings displaced to lower and higher frequencies. If we move the peak to lower frequencies (~80 Hz) with respect to the statistical fitting, the diffusion coefficient will be displaced to higher energies and will increase the diffusion over the energies of interest (square marker in Figure 3b). Therefore, for fixed electron precipitation, moving the peak frequency to lower values results in smaller wave amplitudes compared to the ones provided by the statistical fitting. Since the statistical fitting overestimated the hiss intensity, moving the peak frequency to lower values provides better estimates of the wave amplitude, while moving the peak to higher frequencies further overestimates this amplitude. Similarly, the Gaussian fitting peaks at too high frequencies (550 Hz), which also overestimates the hiss intensity by about a factor of 2. The overall sensitivity of the technique to the frequency spectrum for this event is quite noticeable, with a maximum absolute difference between models of 153 pT but always within a factor of <2.09 with respect to the observed wave amplitude.

The third event is similar to the first one in that its observed frequency spectrum resembles the one captured by statistics. For this reason, not only the observed frequency spectrum but also its statistical model and fitting are capable of accurately reproducing the observed wave amplitude. The observed peak frequency as well as its statistical estimate, however, are much lower than the standard 550 Hz value used in the Gaussian representation. Consequently, the Gaussian fitting and the spectrum displaced to higher frequencies (peak to right) significantly overestimate the hiss intensity for the same reasons described in event 2, since these spectra peak at frequency values that are much higher than the observed or statistical ones. Despite these differences, the ratio of amplitudes remains between 0.84 and 1.71 for any of the input spectrums, and the maximum difference between model outputs is 74 pT.

4.3. Sensitivity to Electron Energy Spectra

The last of the inputs to consider is the electron energy spectrum, whose sensitivity is studied in Table 4. As with density, the observed spectra (from MagEIS data) always provide the most accurate hiss wave amplitudes, and all the input models (including the observed spectra) slightly underestimate the observed wave amplitude. Also, it is clear from Figures 2c, 2f, and 2i that the kappa function is definitely the model that deviates the most from the observed energy spectrum for all three events, since the kappa negative slope is much more pronounced than that of the observed spectra or its statistical representation. Consequently, the kappa function is also the model that provides the worst estimates of the hiss intensity for any of the events, as shown in Table 4. Instead of selecting the optimum values of χ^2 and κ that better reproduce the observed energy spectrum, we purposely selected values that slightly deviate from those optimum parameters (within a reasonable range [*Ni et al.*, 2014b]) with the purpose of testing the sensitivity. Moreover, even in the case of the kappa function, the technique does not seem very sensitive to the electron energy spectrum. For the

Table 4. Sensitivity to Electron Energy Spectra[a]

Event	*E* spectra	Observed B_w (pT)	Inferred B_w (pT)	Difference (pT)	Ratio
1	Observed	119	87	−32	0.73
	Kappa		76	−43	0.64
	Statistical, 25%		83	−36	0.70
	Statistical, median		87	−32	0.73
	Statistical, 75%		85	−34	0.71
2	Observed	121	100	−21	0.83
	Kappa		81	−40	0.67
	Statistical, 25%		89	−32	0.74
	Statistical, median		90	−31	0.75
	Statistical, 75%		89	−32	0.74
3	Observed	85	81	−4	0.95
	Kappa		73	−12	0.86
	Statistical, 25%		80	−5	0.94
	Statistical, median		76	−9	0.89
	Statistical, 75%		79	−6	0.93

[a]Density and wave frequency spectrum set to their observed values.

first event, for example, the inferred wave amplitudes are always within a factor of 0.64–0.73 of the observed value, and the maximum difference between models is only 11 pT. Similarly, the ratio of amplitudes for the second event is always >0.67, and the maximum difference between models is 19 pT. The last event performs even better, with a worst-case ratio of 0.86 for the kappa function and a maximum difference between models of only 8 pT.

5. Discussion and Summary

In this paper we have studied the sensitivity of the POES technique to its different inputs, which has been used to calculate the plasmaspheric hiss intensity. The technique uses POES electron flux data to infer wave amplitudes, which has the advantage of offering a larger coverage in *L* shell and MLT compared to the limited in situ wave observations from other spacecraft; the method could potentially be used to build a global instantaneous model of the plasmaspheric hiss intensity within the technique limitations. The technique provides reliable results when the electron precipitating fluxes are sufficiently high, which may limit its applicability to *L* shells mapping to the outermost part of the plasmasphere; ray tracing techniques, however, could be used to find the wave amplitudes at lower *L* shells from the high *L* shell results using the POES technique [*Bortnik et al.*, 2008, 2009, 2011; *Chen et al.*, 2012a, 2012b]. The inputs to the technique are the cold plasma density, the wave frequency spectra, and the electron energy spectra. In order to demonstrate the sensitivity to these parameters, we selected three conjunction events between the POES and RBSP spacecraft where hiss waves were observed. Subsequently, we used the technique to calculate the inferred wave amplitude for a variety of input models, and we compared the results to the wave observations from the Van Allen Probes. To better isolate the sensitivity to each specific input, we only varied one of them at a time while the other two were set to their observed values averaged over the conjunction bin.

The results show that the technique is most sensitive to the wave frequency spectrum, followed by the cold plasma density. On the other hand, the model for the electron energy spectrum only produces minor changes in the results. Independently of the models used, however, all the estimates always remain within a factor of 0.48 to 2.09 of the observed amplitudes, which is comparable to the scattering between observed and predicted wave amplitudes calculated by *Li et al.* [2014].

The best performance is obtained when the frequency spectrum is set to its observed and statistical values. These statistics are based on Van Allen Probes data from the EMFISIS instruments, which are capable of covering frequencies as low as 20 Hz. This is important because EMFISIS wave observations show that very low frequency hiss features are indeed common, which could not be captured by previous missions like the CRRES spacecraft due to the limited wave frequency coverage. These very low frequency events, however, should

be included in the statistics of the wave frequency spectra for the technique to produce accurate hiss wave amplitude estimates. We have also shown that the standard Gaussian representation of the frequency spectrum centered at 550 Hz performs poorly because its peak frequency is too high; thus, it tends to overestimate the wave amplitudes. Additionally, we have studied the effect of varying the peak frequency of the statistical fitting between ~80 Hz and ~800 Hz; for the same reasons as for the Gaussian distribution, moving the peak frequency to higher values tends to overestimate the hiss intensity, while moving the peak toward lower frequencies works well for the very low frequency hiss events.

Similarly, the density input that produces the most accurate results always corresponds to its observed value. Moreover, in two out of the three events the Sheeley's model (based on the statistical results from the CRRES data) underestimates the measured plasma density. The variation of the density between its statistical bounds produces significant changes in the results; thus, it is important to correctly model this parameter.

Finally, we have shown that the energy spectrum of 100 keV to 300 keV electrons does not significantly modify the outputs of the technique. The best results are always obtained with the observed energy spectrum. However, a kappa function with $\chi^2 = 0.05$ and $\kappa = 5$, which significantly differs from the observed spectrum, also produces good estimates of the hiss wave amplitudes with a factor of 0.64 in the worst of the cases.

The ultimate purpose of the technique is to build a global model of plasmaspheric hiss waves using POES electron observations alone. In general, we will not have the observed plasma density, frequency spectrum, or electron energy spectrum available, which in this paper we took from Van Allen Probes observations. For this reason, it is important to have accurate models in hand for these input parameters and to quantify the errors involved in producing these wave estimates. This study has shown that the statistical representation of the wave frequency spectrum based on EMFISIS data is an accurate assumption for the purposes of the POES technique. Additionally, the model used for the energy spectrum does not have a dominant role; thus, a kappa function would be fine to use, as well as a statistical model based on MagEIS data. In contrast, the plasma density plays a relevant role; the available statistical model based on CRRES data, however, seems to deviate from the observed density in two out of the three events. Although the ratio of amplitudes is not larger than 2.09 for the worst density estimation, new statistical models of the density based on Van Allen Probes data dependent on geomagnetic activity could help in improving the performance of the POES technique. Finally, although not part of this analysis, it must be noted that the implementation of the global hiss model would also require an input model for the plasmapause location, which would be used to distinguish precipitation caused by hiss waves (inside the plasmasphere) from that caused by chorus waves (outside the plasmasphere). This additional input parameter will introduce new uncertainties in the results, which were not present in the analysis of RBSP conjunction events but should be carefully addressed in the future work.

Acknowledgments

M. de Soria-Santacruz acknowledges fellowship support (Jack Eddy Postdoctoral Fellowship) from University Corporation for Atmospheric Research (UCAR). Work at UCLA was supported by JHU/APL contracts 967399 and 921647 under NASA's prime contract NAS5-01072. The analysis at UCLA was supported by the EMFISIS subaward 1001057397:01; ECT subaward 13-041; NASA grants NNX11AD75G, NNX11AR64G, NNX12AD12G, NNX13AI61G, NNX15AF61G, and NNX14AI18G; and NSF GEM grant of AGS-1405054. B. Ni thanks the support from the NSFC grants 41204120 and 41474141 and from the Fundamental Research Funds for the Central Universities grant 2042014kf0251. Work at the University of Iowa was performed under support on JHU/APL contract 921647 under NASA prime contract NAS5-01072. We acknowledge the Van Allen Probes data from the EMFISIS instrument obtained from https://emfisis.physics.uiowa.edu/data/index and from the MagEIS instrument obtained from http://www.rbsp-ect.lanl.gov/data_pub/. We also would like to thank the NOAA POES team especially Janet Green for providing the NOAA POES data (obtained from http://satdat.ngdc.noaa.gov/sem/poes/data/) and helpful advice on the use of the data.

Michael W. Liemohn thanks the reviewers for their assistance in evaluating this paper.

References

Abel, B., and R. M. Thorne (1998), Electron scattering loss in Earth's inner magnetosphere: 1. Dominant physical processes, *J. Geophys. Res.*, *103*(A2), 2385–2396, doi:10.1029/97JA02919.

Baker, D. N., S. G. Kanekal, R. B. Horne, N. P. Meredith, and S. A. Glauert (2007), Low-altitude measurements of 2–6 MeV electron trapping lifetimes at $1.5 \leq L \geq 2.5$, *Geophys. Res. Lett.*, *34*, L20110, doi:10.1029/2007GL031007.

Blake, J. B., et al. (2013), The Magnetic Electron Ion Spectrometer (MagEIS) instruments aboard the Radiation Belt Storm Probes (RBSP) spacecraft, *Space Sci. Rev.*, *179*(1–4), 383–421, doi:10.1007/s11214-013-9991-8.

Bortnik, J., R. M. Thorne, and N. P. Meredith (2008), The unexpected origin of plasmaspheric hiss from discrete chorus emissions, *Nature*, *452*(7183), 62–66, doi:10.1038/nature06741.

Bortnik, J., W. Li, R. M. Thorne, V. Angelopoulos, C. Cully, J. Bonnell, O. Le Contel, and A. Roux (2009), An observation linking the origin of plasmaspheric hiss to discrete chorus emissions, *Science*, *324*(5928), 775–778, doi:10.1126/science.1171273.

Bortnik, J., L. Chen, W. Li, R. M. Thorne, N. P. Meredith, and R. B. Horne (2011), Modeling the wave power distribution and characteristics of plasmaspheric hiss, *J. Geophys. Res.*, *116*, A12209, doi:10.1029/2011JA016862.

Chen, L., J. Bortnik, W. Li, R. M. Thorne, and R. B. Horne (2012a), Modeling the properties of plasmaspheric hiss: 1. Dependence on chorus wave emission, *J. Geophys. Res.*, *117*, A05201, doi:10.1029/2011JA017201.

Chen, L., J. Bortnik, W. Li, R. M. Thorne, and R. B. Horne (2012b), Modeling the properties of plasmaspheric hiss: 2. Dependence on the plasma density distribution, *J. Geophys. Res.*, *117*, A05202, doi:10.1029/2011JA017202.

Chen, L., et al. (2014a), Generation of unusually low frequency plasmaspheric hiss, *Geophys. Res. Lett.*, *41*, 5702–5709, doi:10.1002/2014GL060628.

Chen, Y., G. D. Reeves, R. H. W. Friedel, and G. S. Cunningham (2014b), Global time-dependent chorus maps from low-Earth-orbit electron precipitation and Van Allen Probes data, *Geophys. Res. Lett.*, *41*, 755–761, doi:10.1002/2013GL059181.

Horne, R. B., R. M. Thorne, S. A. Glauert, N. P. Meredith, D. Pokhotelov, and O. Santolík (2007), Electron acceleration in the Van Allen radiation belts by fast magnetosonic waves, *Geophys. Res. Lett.*, *34*, L17107, doi:10.1029/2007GL030267.

Kennel, C. F., and H. E. Petschek (1966), Limit on stably trapped particle fluxes, *J. Geophys. Res.*, *71*(1), 1–28.

Kletzing, C. A., et al. (2014), The Electric and Magnetic Field Instrument Suite and Integrated Science (EMFISIS) on RBSP, in *The Van Allen Probes Mission*, edited by N. Fox and J. L. Burch, pp. 127–181, Springer, New York.

Kurth, W. S., S. De Pascuale, J. B. Faden, C. A. Kletzing, G. B. Hospodarsky, S. Thaller, and J. R. Wygant (2015), Electron densities inferred from plasma wave spectra obtained by the waves instrument on Van Allen Probes, *J. Geophys. Res. Space Physics*, *120*, 904–914, doi:10.1002/2014JA020857.

Li, W., R. M. Thorne, J. Bortnik, Y. Nishimura, V. Angelopoulos, L. Chen, J. P. McFadden, and J. W. Bonnell (2010), Global distributions of suprathermal electrons observed on THEMIS and potential mechanisms for access into the plasmasphere, *J. Geophys. Res.*, *115*, A00J10, doi:10.1029/2010JA015687.

Li, W., B. Ni, R. M. Thorne, J. Bortnik, J. C. Green, C. A. Kletzing, W. S. Kurth, and G. B. Hospodarsky (2013a), Constructing the global distribution of chorus wave intensity using measurements of electrons by the POES satellites and waves by the Van Allen Probes, *Geophys. Res. Lett.*, *40*, 4526–4532, doi:10.1002/grl.50920.

Li, W., et al. (2013b), An unusual enhancement of low-frequency plasmaspheric hiss in the outer plasmasphere associated with substorm-injected electrons, *Geophys. Res. Lett.*, *40*, 3798–3803, doi:10.1002/grl.50787.

Li, W., et al. (2014), Quantifying hiss-driven energetic electron precipitation: A detailed conjunction event analysis, *Geophys. Res. Lett.*, *41*, 1085–1092, doi:10.1002/2013GL059132.

Li, W., Q. Ma, R. M. Thorne, J. Bortnik, C. A. Kletzing, W. S. Kurth, G. B. Hospodarsky, and Y. Nishimura (2015), Statistical properties of plasmaspheric hiss derived from Van Allen Probes data and their effects on radiation belt electron dynamics, *J. Geophys. Res. Space Physics*, *120*, doi:10.1002/2015JA021048.

Lyons, L. R., and R. M. Thorne (1973), Equilibrium structure of radiation belt electrons, *J. Geophys. Res.*, *78*(13), 2142–2149, doi:10.1029/JA078i013p02142.

Meredith, N. P., R. B. Horne, R. M. Thorne, D. Summers, and R. R. Anderson (2004), Substorm dependence of plasmaspheric hiss, *J. Geophys. Res.*, *109*, A06209, doi:10.1029/2004JA010387.

Meredith, N. P., R. B. Horne, S. A. Glauert, R. M. Thorne, D. Summers, J. M. Albert, and R. R. Anderson (2006), Energetic outer zone electron loss timescales during low geomagnetic activity, *J. Geophys. Res.*, *111*, A05212, doi:10.1029/2005JA011516.

Meredith, N. P., R. B. Horne, S. A. Glauert, and R. R. Anderson (2007), Slot region electron loss timescales due to plasmaspheric hiss and lightning-generated whistlers, *J. Geophys. Res.*, *112*, A08214, doi:10.1029/2007JA012413.

Meredith, N. P., R. B. Horne, S. A. Glauert, D. N. Baker, S. G. Kanekal, and J. M. Albert (2009), Relativistic electron loss timescales in the slot region, *J. Geophys. Res.*, *114*, A03222, doi:10.1029/2008JA013889.

Meredith, N. P., R. B. Horne, M. M. Lam, M. H. Denton, J. E. Borovsky, and J. C. Green (2011), Energetic electron precipitation during high-speed solar wind stream driven storms, *J. Geophys. Res.*, *116*, A05223, doi:10.1029/2010JA016293.

Ni, B., R. M. Thorne, Y. Y. Shprits, and J. Bortnik (2008), Resonant scattering of plasma sheet electrons by whistler-mode chorus: Contribution to diffuse auroral precipitation, *Geophys. Res. Lett.*, *35*, L11106, doi:10.1029/2008GL034032.

Ni, B., R. M. Thorne, N. P. Meredith, R. B. Horne, and Y. Y. Shprits (2011), Resonant scattering of plasma sheet electrons leading to diffuse auroral precipitation: 2. Evaluation for whistler mode chorus waves, *J. Geophys. Res.*, *116*, A04219, doi:10.1029/2010JA016233.

Ni, B., J. Bortnik, R. M. Thorne, Q. Ma, and L. Chen (2013), Resonant scattering and resultant pitch angle evolution of relativistic electrons by plasmaspheric hiss, *J. Geophys. Res. Space Physics*, *118*, 7740–7751, doi:10.1002/2013JA019260.

Ni, B., et al. (2014a), Resonant scattering of energetic electrons by unusual low-frequency hiss, *Geophys. Res. Lett.*, *41*, 1854–1861, doi:10.1002/2014GL059389.

Ni, B., W. Li, R. M. Thorne, J. Bortnik, J. C. Green, C. A. Kletzing, W. S. Kurth, G. B. Hospodarsky, and M. Soria-Santacruz Pich (2014b), A novel technique to construct the global distribution of whistler mode chorus wave intensity using low-altitude POES electron data, *J. Geophys. Res. Space Physics*, *119*, 5685–5699, doi:10.1002/2014JA019935.

Orlova, K., M. Spasojevic, and Y. Shprits (2014), Activity-dependent global model of electron loss inside the plasmasphere, *Geophys. Res. Lett.*, *41*, 3744–3751, doi:10.1002/2014GL060100.

Parrot, M., and F. Lefeuvre (1986), Statistical study of the propagation characteristics of ELF hiss observed on GEOS-1, inside and outside the plasmasphere, *Ann. Geosphys.*, *4*(5), 363–384.

Rodger, C. J., M. A. Clilverd, J. C. Green, and M. M. Lam (2010), Use of POES SEM-2 observations to examine radiation belt dynamics and energetic electron precipitation into the atmosphere, *J. Geophys. Res.*, *115*, A04202, doi:10.1029/2008JA014023.

Santolik, O., M. Parrot, L. R. O. Storey, J. S. Pickett, and D. A. Gurnett (2001), Propagation analysis of plasmaspheric hiss using Polar PWI measurements, *Geophys. Res. Lett.*, *28*(6), 1127–1130, doi:10.1029/2000GL012239.

Santolik, O., M. Parrot, and F. Lefeuvre (2003), Singular value decomposition methods for wave propagation analysis, *Radio Sci.*, *38*(1), 1010, doi:10.1029/2000RS002523.

Sheeley, B. W., M. B. Moldwin, H. K. Rassoul, and R. R. Anderson (2001), An empirical plasmasphere and trough density model: CRRES observations, *J. Geophys. Res.*, *106*(A11), 25,631–25,641.

Spence, H. E., et al. (2013), Science goals and overview of the Energetic Particle, Composition, and Thermal Plasma (ECT) suite on NASA's Radiation Belt Storm Probes (RBSP) Mission, *Space Sci. Rev.*, *179*, 311–336, doi:10.1007/s11214-013-0007-5.

Summers, D., B. Ni, N. P. Meredith, R. B. Horne, R. M. Thorne, M. B. Moldwin, and R. R. Anderson (2008), Electron scattering by whistler-mode ELF hiss in plasmaspheric plumes, *J. Geophys. Res.*, *113*, A04219, doi:10.1029/2007JA012678.

Thorne, R. M., E. J. Smith, R. K. Burton, and R. E. Holzer (1973), Plasmaspheric hiss, *J. Geophys. Res.*, *78*(10), 1581–1596, doi:10.1029/JA078i010p01581.

Thorne, R. M., et al. (2013), Evolution and slow decay of an unusual narrow ring of relativistic electrons near l~ 3.2 following the september 2012 magnetic storm, *Geophys. Res. Lett.*, *40*, 3507–3511, doi:10.1002/grl.50627.

Xiao, F., C. Shen, Y. Wang, H. Zheng, and S. Wang (2008), Energetic electron distributions fitted with a relativistic kappa-type function at geosynchronous orbit, *J. Geophys. Res.*, *113*, A05203, doi:10.1029/2007JA012903.

Zhao, H., and X. Li (2013), Modeling energetic electron penetration into the slot region and inner radiation belt, *J. Geophys. Res. Space Physics*, *118*, 6936–6945, doi:10.1002/2013JA019240.